

## CHAPTER 6

### Inversion of Seismic Data

#### 6.1 Introduction

Seismic inversion theoretically means to extract quantitative rock properties from the reflection of seismic data. This process is to recover the lost component of seismic at high and low frequencies, “it increases the resolution of conventional seismic in many cases and puts the study of reservoir parameters at different level” (Veeken and Silva, 2004). Inversion traditionally has been applied for post-stack seismic dataset, with the objective of extracting acoustic impedance (AI) volumes. AI is defined as a rock property and estimated by multiplication of P-wave velocity ( $V_p$ ) and density ( $\rho$ ) log of the rock:

$$Z (AI) = V_p \times \rho. \quad (6.1)$$

Acoustic impedance inversion in present days has become integrating study of many interpretation projects to enhance understanding about reservoir characterization. However, there is an important limitation of acoustic impedance inversion that it just runs on full stack seismic data therefore ignoring any AVO effects. Seismic reflection amplitude varies with offset or angle (AVO) represents differences in lithology type and fluid contents above and below the reflectors. Nowadays, with increasing knowledge became apparent that AVO needed to account for in inversion seismic data. Therefore, it is necessary to create a type of inversion that can incorporate AVO into seismic inversion.

In the study area, acoustic impedance values of the gas-bearing sand reservoirs are nearly similar to the acoustic impedance values of surrounding shale, this leads to difficulty in distinguishing between the reservoirs and surrounding shale in full stack seismic volume. Fortunately, pre-stack migrated seismic dataset is provided by the company. After considering the amplitude variations with angles in seismic CMP

gathers, the gas saturated reservoirs are easier to identify in far angles in the seismic data. Thus, the pre-stack impedance inversion needs to be carried out.

For the above reasons, elastic impedance (EI) inversion was presented by Patrick Connolly in 1999. It is a generalization of acoustic impedance for variable incidence angle (Connolly, 1999). The EI inversion allows inverted non-normal offset or incidence angle seismic data same as AI inversion with the zero offset or angle volume. The EI approximation is derived from linear Zoeppritz equations (Equation 6.2).

$$R(\theta) = A + B\sin^2\theta + C\sin^2\theta\tan^2\theta, \quad (6.2)$$

where

$$A = \frac{1}{2} \left( \frac{\Delta V_P}{V_P} + \frac{\Delta \rho}{\rho} \right),$$

$$B = \frac{\Delta V_P}{2V_P} - 4 \frac{V_S^2}{V_P^2} \frac{\Delta V_S}{V_S} - 2 \frac{V_S^2}{V_P^2} \frac{\Delta \rho}{\rho},$$

$$C = \frac{1}{2} \frac{\Delta V_P}{V_P}.$$

The main parameters in EI functions are elastic parameters of rocks: P-wave velocity, S-wave velocity, density and incidence angle  $\theta$ . The EI approximation is shown as:

$$EI(\theta) = V_P^a * V_S^b * \rho^c, \quad (6.3)$$

where

$$a = 1 + \tan^2\theta,$$

$$b = -8K\sin^2\theta,$$

$$c = 1 - 4K\sin^2\theta,$$

$$K = \left( \frac{V_S}{V_P} \right)^2.$$

## 6.2 Elastic Impedance Log Generation

Before inversion process, the elastic impedance logs which are EI\_near, EI\_mid and EI\_far are created at 6.5 degrees, 19.5 degrees and 33 degrees respectively (Figure 6.1). These EI logs are calculated by Equation 6.3 for different incidence angles. It is obvious that three EI logs near, mid and far are similar in appearance, but the value ranges of them are different. With increasing incidence angle, the level of EI log decreases (Connolly, 1999). In the UMA15 reservoir interval (from 2999.1 m to 3014.4 m), there

is enormous decrease in the EI\_far curve while just slight decrease in the EI\_near in the sand reservoir in comparison with surrounding shale. In the MMF30 reservoir interval (from 3583 m to 3616 m), there is a slight decrease in the EI\_far but noticeable increase in the EI\_near and the EI\_mid in the sand reservoir in comparison with surrounding shale.

Figure 6.2 shows the plot of the EI\_near, the EI\_mid and the EI\_far curves together in the same track. In general, the EI\_far is in the right part of the track (EI values increase from left to right) and quite separates with the EI\_mid and the EI\_near which are close together throughout depth of the well A. Nevertheless, notice that the EI\_far log moves closer to the EI\_mid and the EI\_near in the UMA15 reservoir interval, for MMF30 reservoir interval, the EI\_far curve even surpasses to the left of the EI\_mid and the EI\_near curve compares with the EI\_far above and under the reservoir interval where is dominated by shale. These changes in the reservoir intervals are caused by AVO effects between the EI logs.

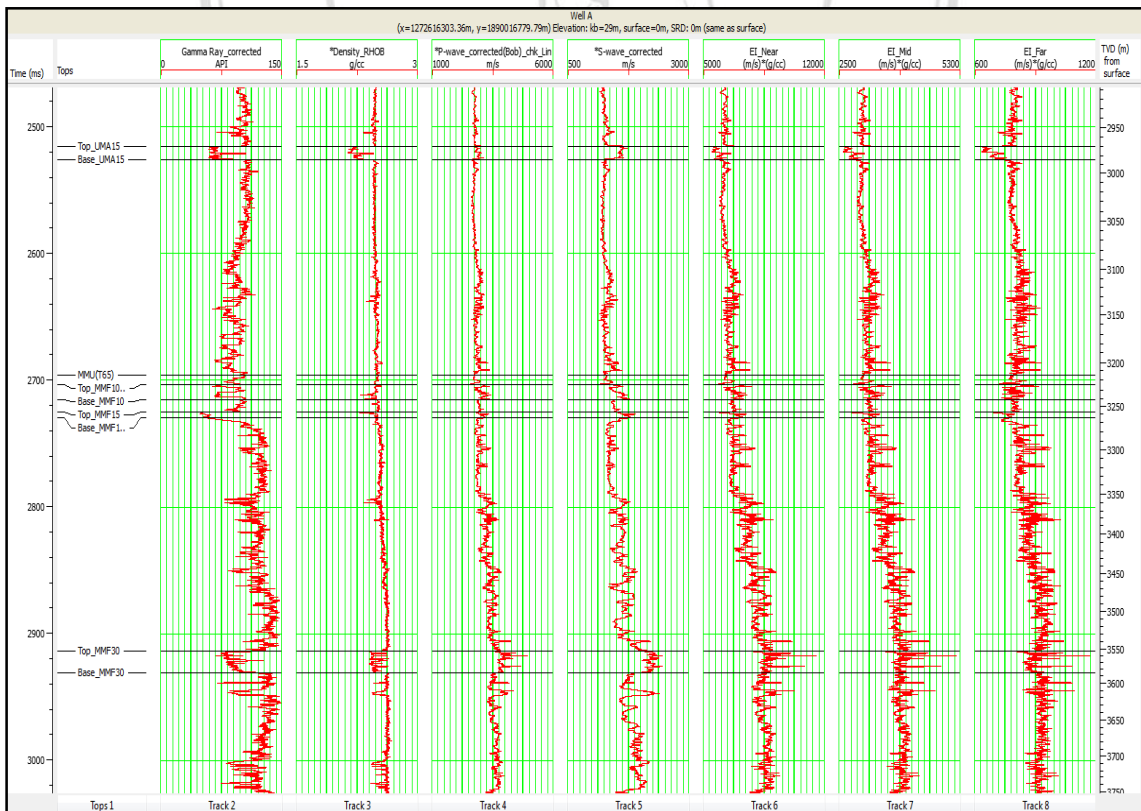


Figure 6.1: Near, mid and far elastic impedance logs. (from left to right) Gamma Ray, Density, P-wave velocity, S-wave velocity, EI\_near, EI\_mid and EI\_far.

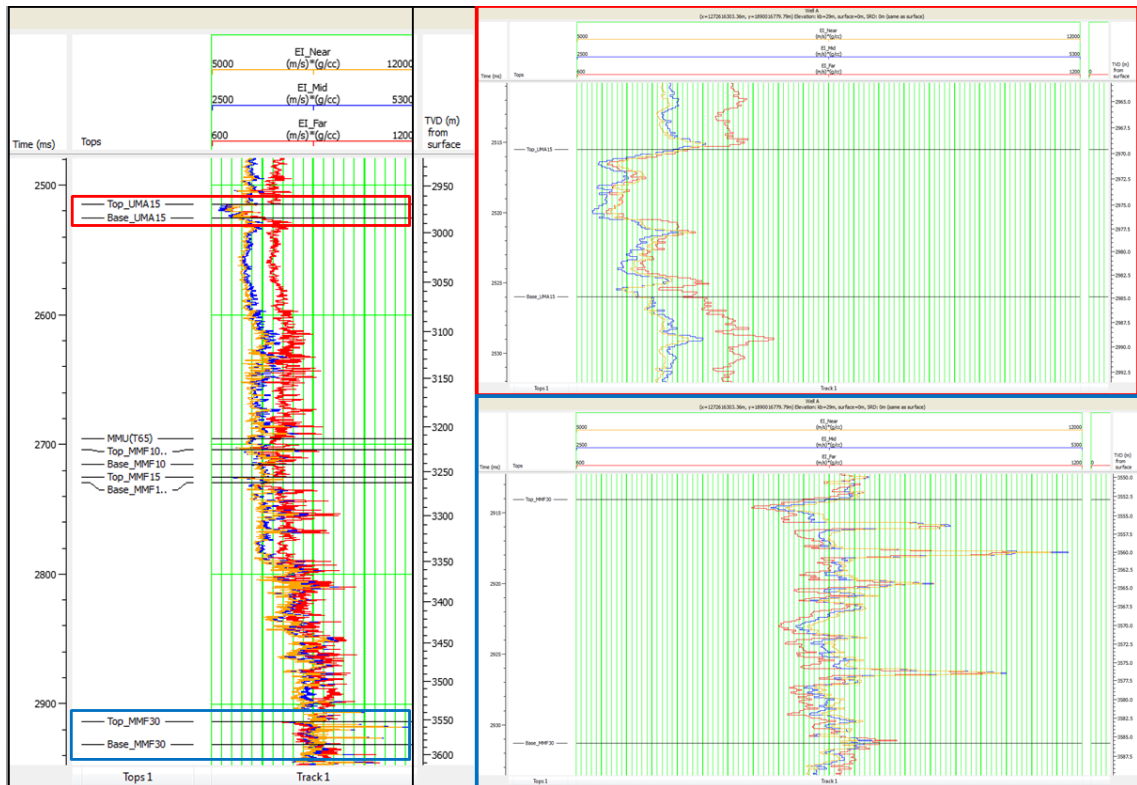


Figure 6.2: Plot of EI\_near (in yellow), EI\_mid (in blue) and EI\_far (in red) curve on the same track. The red rectangle represents the UMA15 reservoir interval and the blue rectangle represents the MMF30 reservoir interval.

In the Well A, the UMA15 sand has AVO class 2 while the MMF30 sand has AVO class 2P (Figures 5.18 and 5.17), so the amplitudes of the UMA15 sand are higher at far angle than at normal incidence angle and the amplitudes of the MMF30 sand are slightly higher at far angle but in reverse polarity than at normal incidence angle. This leads to the discrepancy in expression of the EI logs in the reservoirs intervals. This discrepancy in AVO responses between two reservoirs is more clearly when plotting scaled EI\_far with the acoustic impedance (AI) (Figure 6.3). Because the EI\_far has different level compared to the AI, the EI\_far has to be scaled to plot it overlap AI. It is obvious that the scaled EI\_far has the same shale baseline as the AI log but in the dominated sand intervals the scaled EI\_far and AI are very separately. The difference in AVO class between two sand reservoirs causes the separation between the EI\_far and AI for the UMA15 reservoir is clearer than for the MMF30 reservoir.

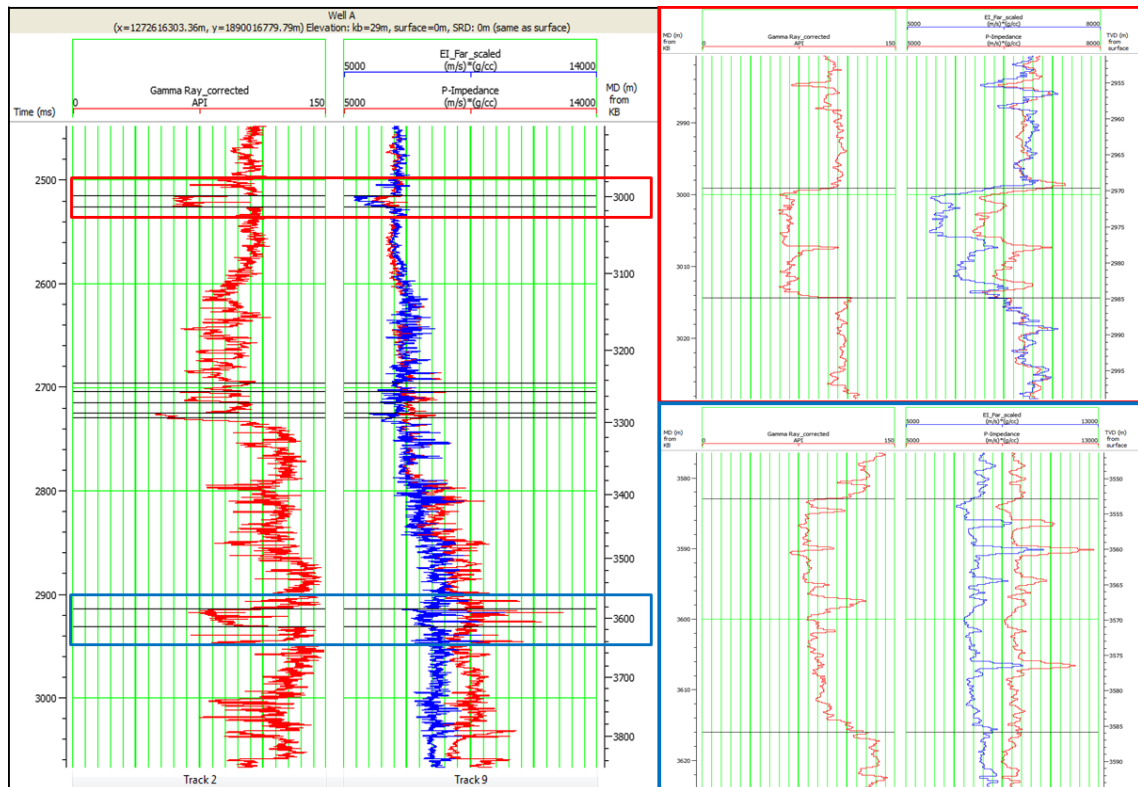


Figure 6.3: Plot of scaled EI\_far curve (in blue) with AI curve (in red). The red rectangle represents the UMA15 reservoir interval and the blue rectangle represents the MMF30 reservoir interval.

### 6.3 Elastic Impedance Inversion

The workflow for elastic impedance inversion used in this study is shown in Figure 6.4, some major steps are done and mentioned in above chapters. The first step which is generating near, mid and far angle stacks is mentioned in part 1 of chapter 5. The second step correlating offset synthetic to the angle stacks and the third step extracting wavelet for inversion are illustrated in part 2 of chapter 5. Next step which is generating EI logs for each angle ranges has been illustrated above in this chapter. After that the EI logs are plotted to find AVO anomalies zones. Next phase is model based inversion for angle stacks to create EI volumes for the different angle ranges. It is followed by cross plotting the different EI volumes against each other to identify AVO anomalies. These zones of AVO anomalies are then highlighted to identify the potential prospects in the study area. After all, the results are integrated to achieve lithology and fluid contents information of the reservoirs.

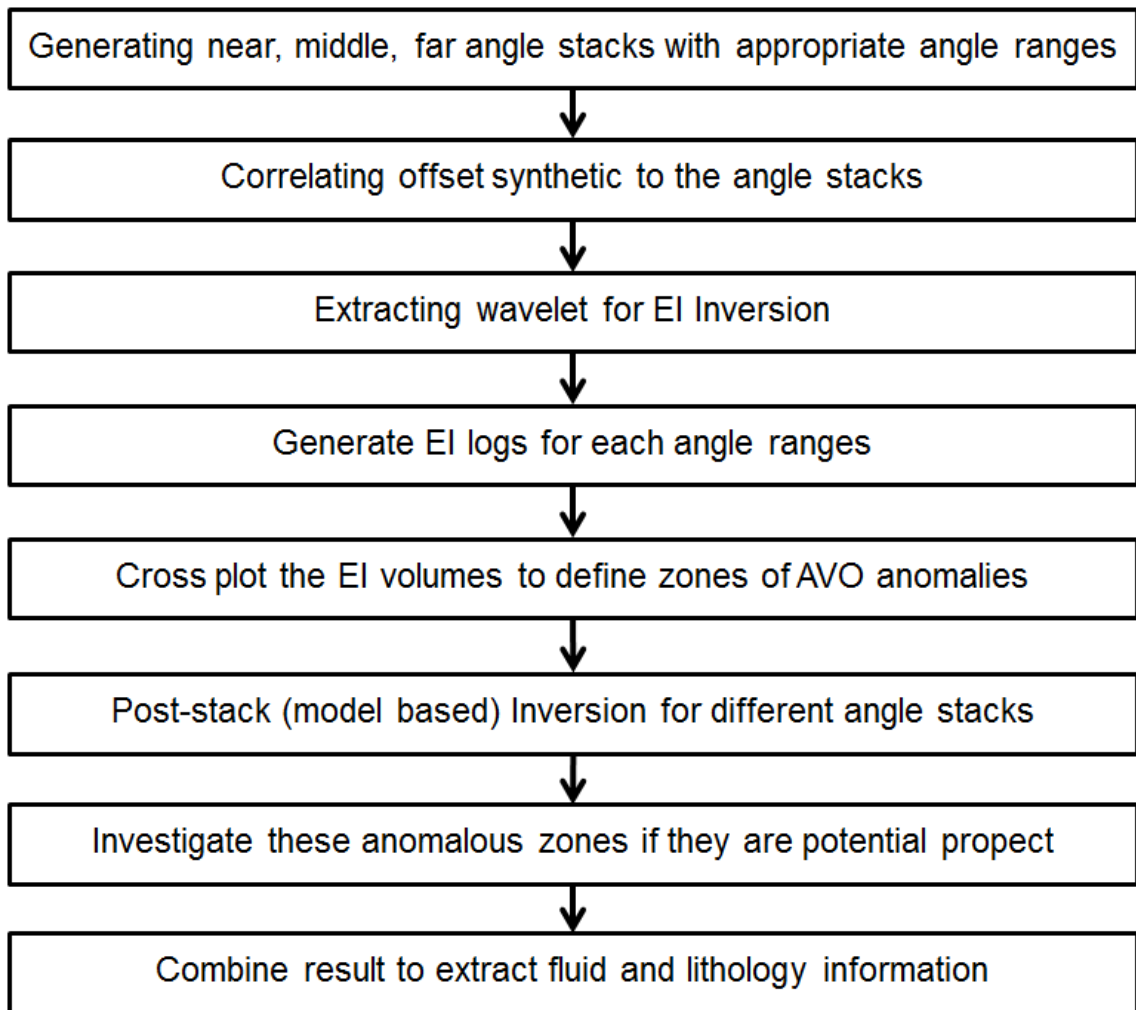


Figure 6.4: Elastic Impedance inversion workflow.

After the EI logs are generated, it is essential to cross plot the EI logs curve against each other in order to see whether zone of interest could be differentiate by angle ranges. This method is used normally for identify zones that have AVO anomalies. The EI logs are cross plotted for two depth intervals that cover each reservoir, from 2900 m to 3100 m for the UMA15 reservoir and from 3500 m to 3700 m for the MMF30 reservoir. Gamma ray log is used as color ranges for log data. Figures 6.5 to 6.7 show the cross plots of the EI\_near and EI\_mid, EI\_near and EI\_far, EI\_mid and EI\_far of the UMA15 reservoir accordingly. Meanwhile, Figures 6.8 to 6.10 show the cross plots of the EI\_near and EI\_mid, EI\_near and EI\_far, EI\_mid and EI\_far of the MMF30 respectively.

In the cross plots for UMA15 reservoir (Figures 6.5 to 6.7), it is clearly that there are two different trends which were highlighted by the red polygons and the blue polygons.

The lower trend (red polygon) may represent the prospect while the upper trend (blue polygon) may represent the outside interval of the prospect. Besides, the lower trend also typically contains low Gamma Ray log data around 60 to 120 API while the upper trend contains high Gamma Ray values above 120 API. When plotting the log data in the cross section through the depth of the well, two zones are indicated very clearly that the red zone is just in the UMA15 reservoir, the rest of the log is covered by the blue zone. Therefore, the blue zone represents normal AVO trend while the red zone indicates AVO anomalies trend.

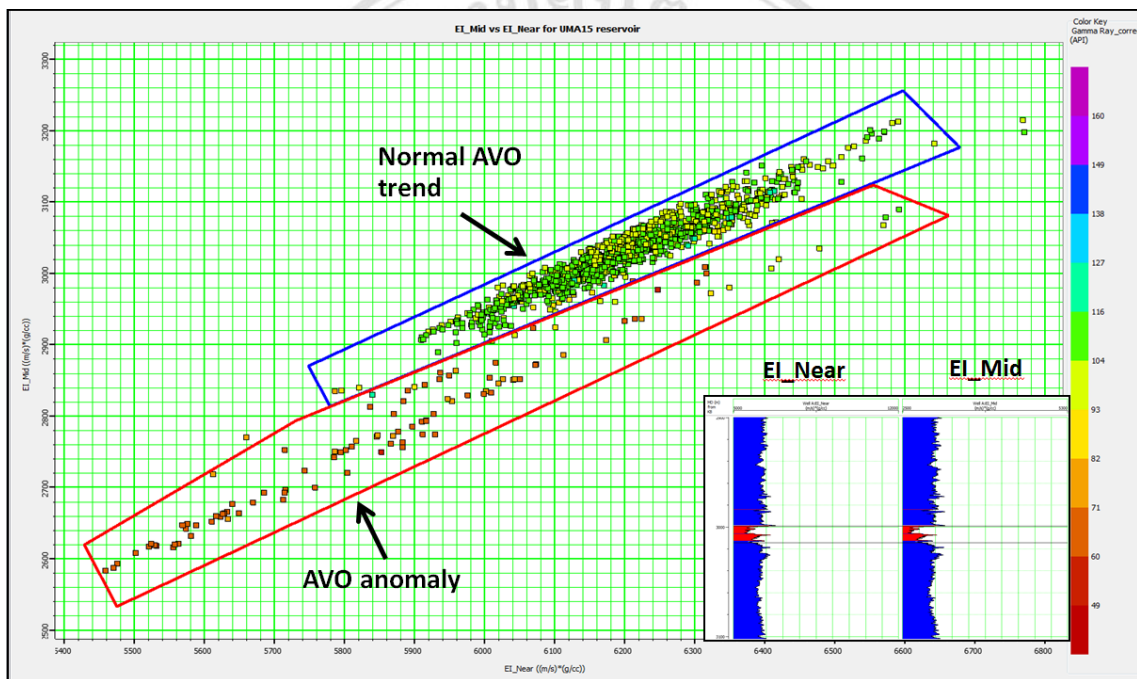


Figure 6.5: Cross plot of EI\_near and EI\_mid for UMA15 reservoir. The blue polygons represents normal AVO trend while the red polygons represents AVO anomalies trend.

The cross section through the well is in the small figure in the right hand side.



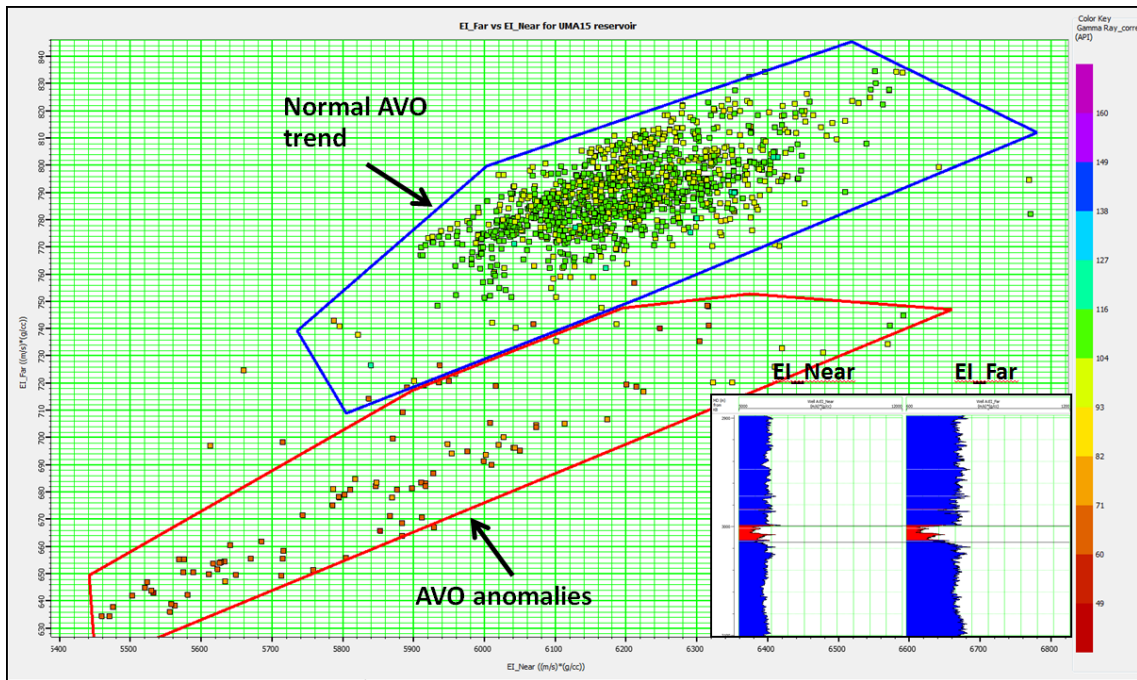


Figure 6.6: Cross plot of EI\_near and EI\_far for UMA15 reservoir. The blue polygons represents normal AVO trend while the red polygons represents AVO anomalies trend.

The cross section through the well is in the small figure in the right hand side.

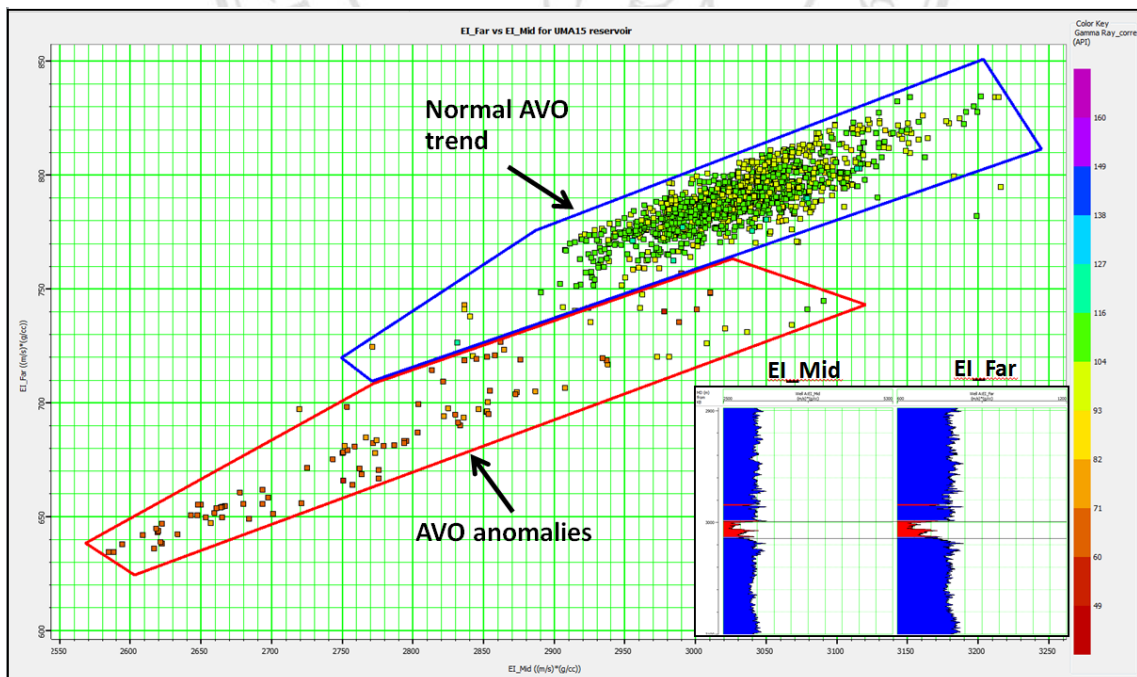


Figure 6.7: Cross plot of EI\_mid and EI\_far for UMA15 reservoir. The blue polygons represents normal AVO trend while the red polygons represents AVO anomalies trend.

The cross section through the well is in the small figure in the right hand side.



In the cross plots for MMF30 reservoir (Figures 6.8 to 6.10), it is obvious that there are also two different trends which were highlighted by the red polygons and the blue polygons. The lower trend (red polygon) may represent the prospect while the upper trend (blue polygon) may represent the outside interval of the prospect. In addition, the lower trend also typically contains low gamma ray log data around 70 to 120 API while the upper trend contains high gamma ray values above 120 API. When plotting the log data in the cross section through the depth of the well, two zones are indicated quite clearly that the red zone is just in the MMF30 reservoir and a very thin sand stone at 3655 m, the rest of the log is covered by the blue zone. Therefore, the blue zone represents shale which have normal AVO trend while the red zone indicates sandstone reservoir which has AVO anomalies trend.

In general the AVO anomalies trend in the MMF30 reservoir is harder to distinguish with the normal trend in comparison with the UMA15 reservoir due to the difference in AVO classes between two reservoirs. Both of two polygons (red and blue) of each cross plots are kept for highlighting amplitude anomalies in the seismic section later in this chapter.

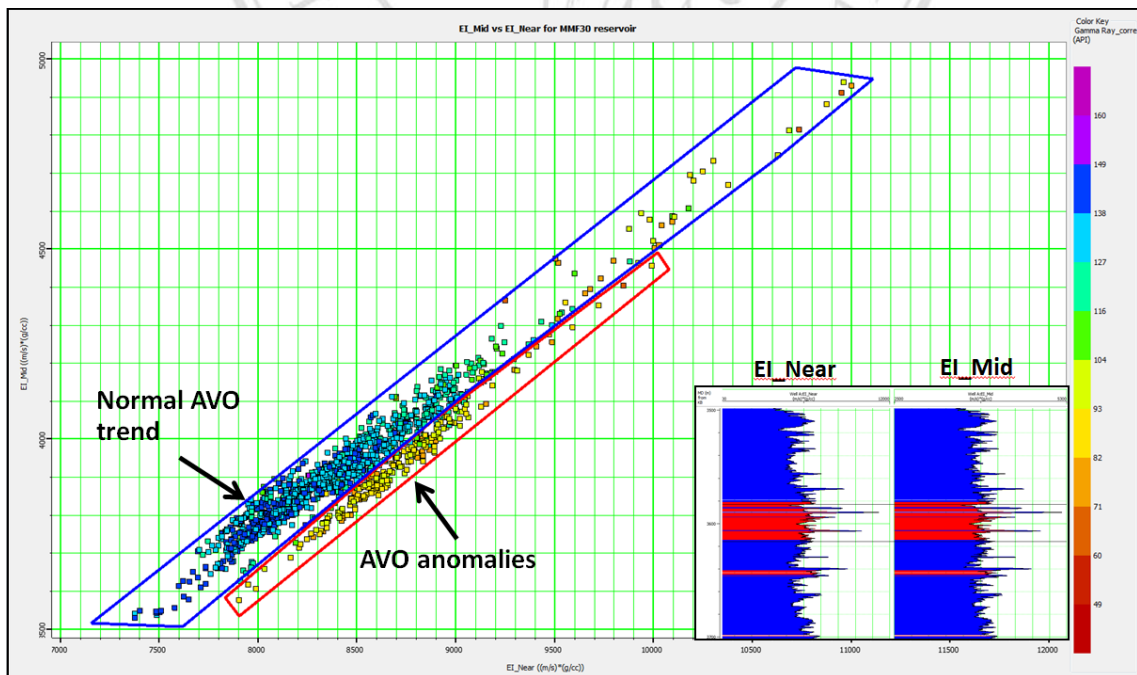


Figure 6.8: Cross plot of EI\_near and EI\_mid for MMF30 reservoir. The blue polygons represents normal AVO trend while the red polygons represents AVO anomalies trend.

The cross section through the well is in the small figure in the right hand side.

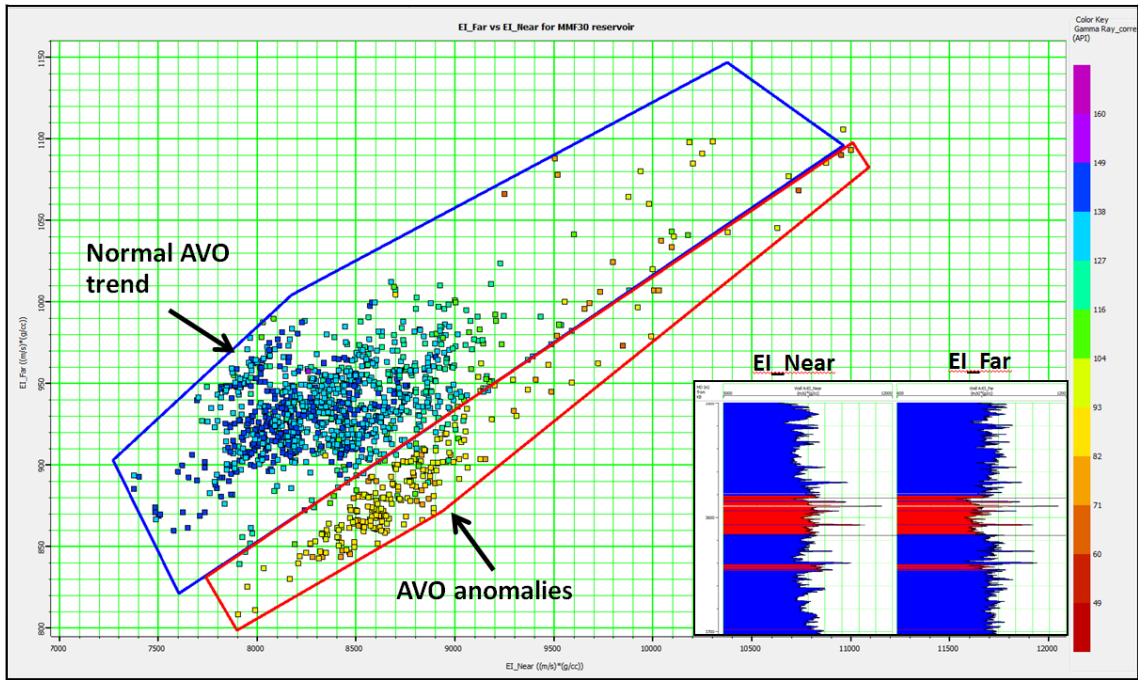


Figure 6.9: Cross plot of EI\_near and EI\_far for MMF30 reservoir. The blue polygons represents normal AVO trend while the red polygons represents AVO anomalies trend. The cross section through the well is in the small figure in the right hand side.

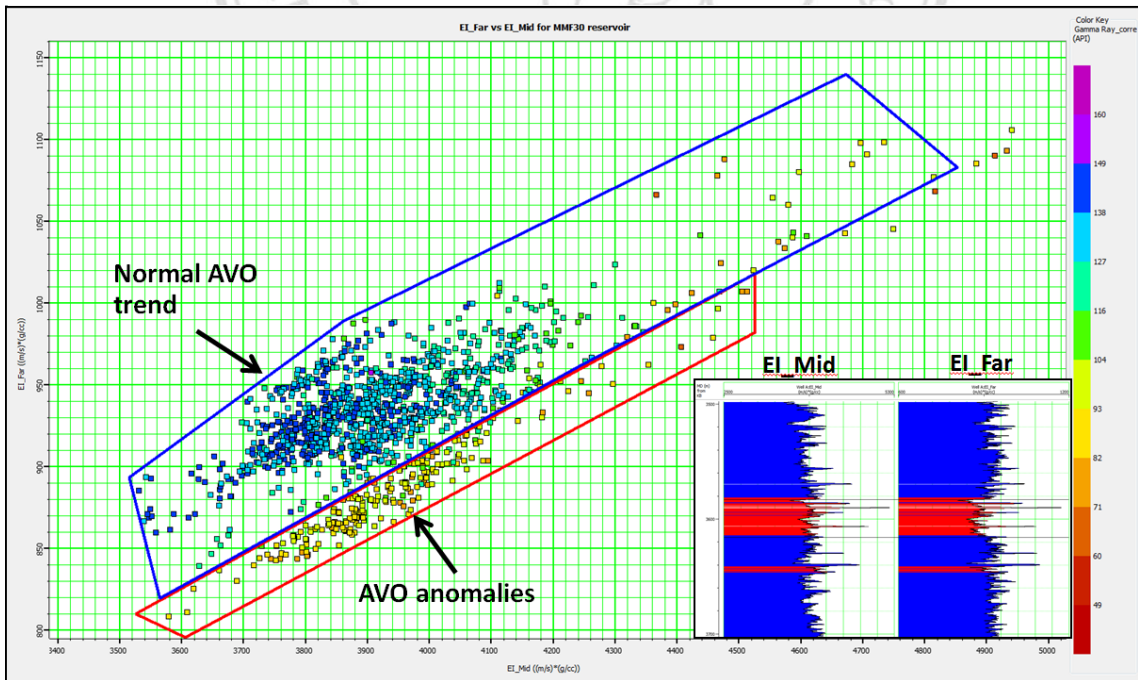


Figure 6.10: Cross plot of EI\_mid and EI\_far for MMF30 reservoir. The blue polygons represents normal AVO trend while the red polygons represents AVO anomalies trend. The cross section through the well is in the small figure in the right hand side.

In this study, the near, mid and far angle stacks are generated with angle ranges of 0 – 13 degrees, 13 – 26 degrees and 26 – 40 degrees respectively. The wavelets used for elastic impedance (EI) inversion are extracted after well to seismic tie for each angle stacks (Figure 5.13). The well to seismic tie process is mentioned in chapter 5. Post stack (model based) inversion are then applied for near, mid and far angle stacks.

The model based inversion process needs an initial strata model first before inverting it to achieve the inverted model. A strata model is a volume defining an interpreted seismic parameter, such as velocity reflectivity or impedance. It tries to define the study area in more geological way by using rock properties term than just as seismic reflectors. For this study, the initial models define the impedance seismic parameter, so the initial impedance models would be built. The initial model requires four log curves which are P-wave velocity after well to seismic tie for each angle stack with the determined time depth function, S-wave velocity, density and elastic impedance  $\log(EI)$  of near, mid and far angle stack. The horizons and faults are also included in the initial model to help interpolation the impedance for the whole volume. Three initial models built for near, mid and far angle stacks are shown from Figures 6.12 to 6.14 respectively.

The initial strata model is a low frequency model, the high frequency detail model can influence the final inversion result negatively (Sams and Saussus, 2013). However, Hampson Russell software (HRS-9) often produces high frequency models by default (high cut frequency 10/15 Hz). Therefore, low pass frequency filters are applied to the model which is 7/11 Hz, 6/11 Hz and 4/10 Hz for the near, mid and far angle stack initial models accordingly (Figure 6.11), this means passing all frequencies up to 7 Hz, 6 Hz and 4 Hz respectively for each angle stack initial models (near, mid and far). The results are in lower detail and more useable for inversion (Figures 6.12 to 6.14).

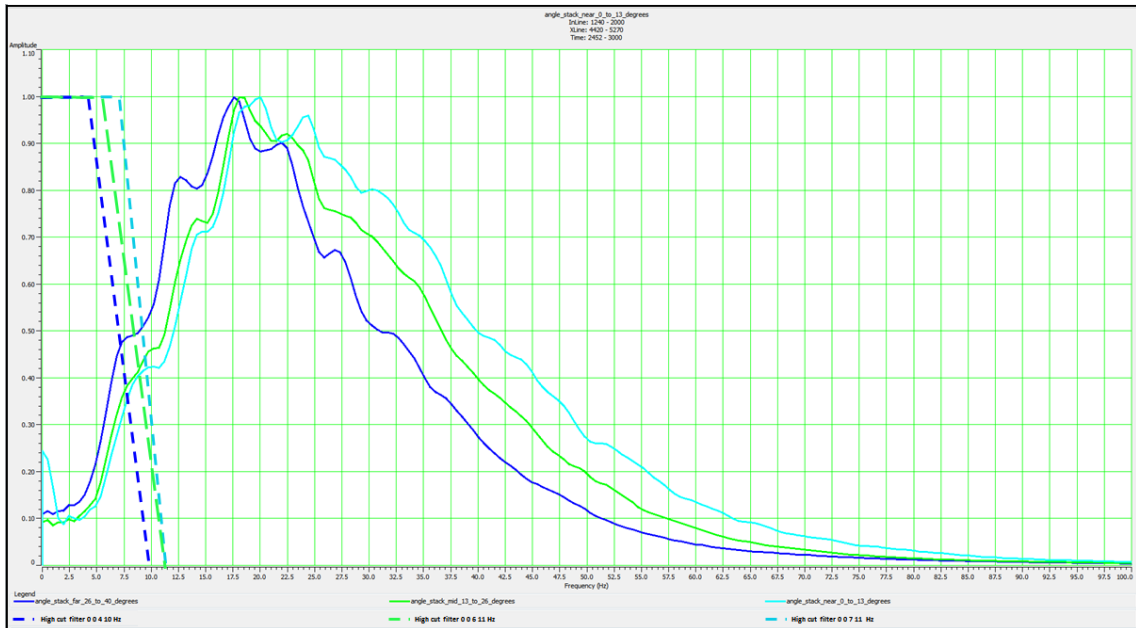


Figure 6.11: Amplitude spectrum of near, mid and far angle stacks from 2450 to 3000 ms (zone of interest) and applied filters for each angle stacks initial model.

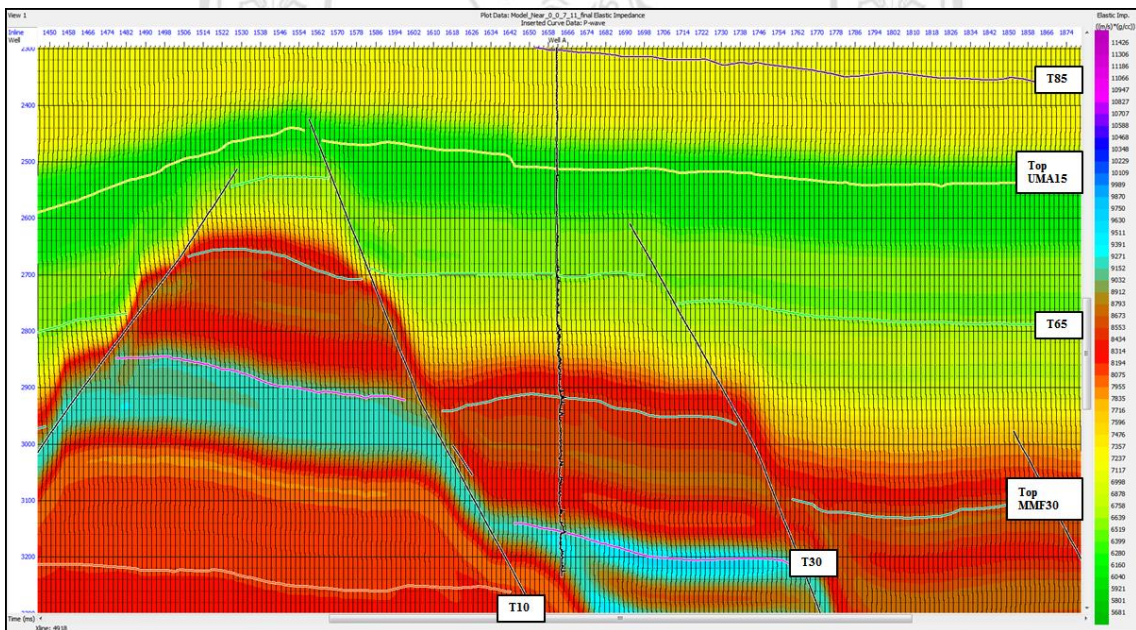


Figure 6.12: Initial strata model for near angle stack (Xline 4918).



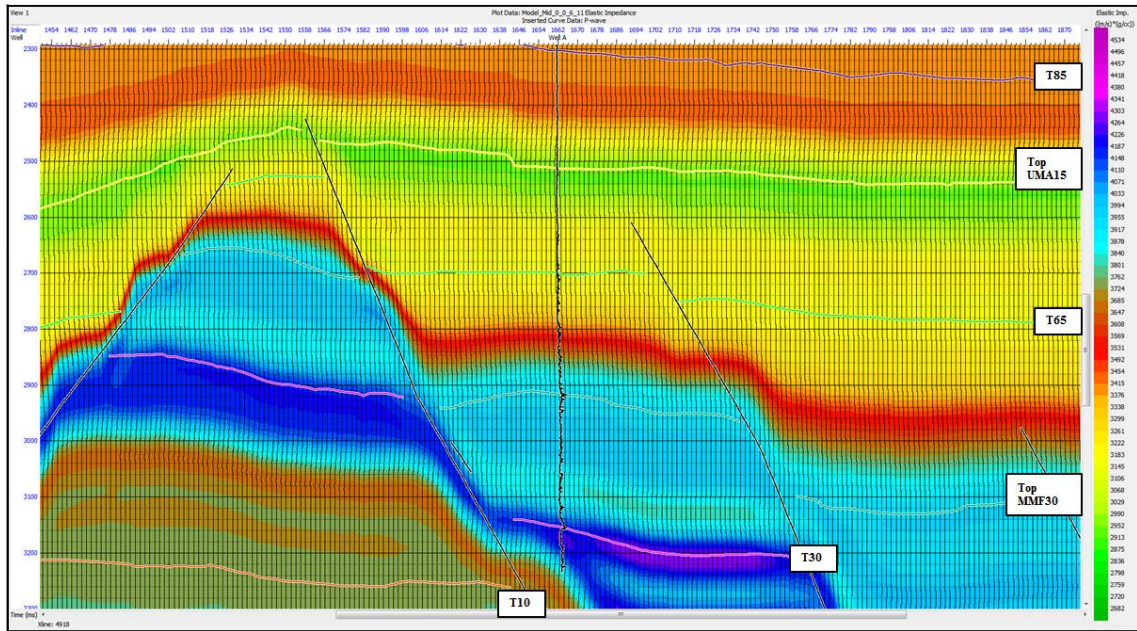


Figure 6.13: Initial strata model for mid angle stack (Xline 4918).

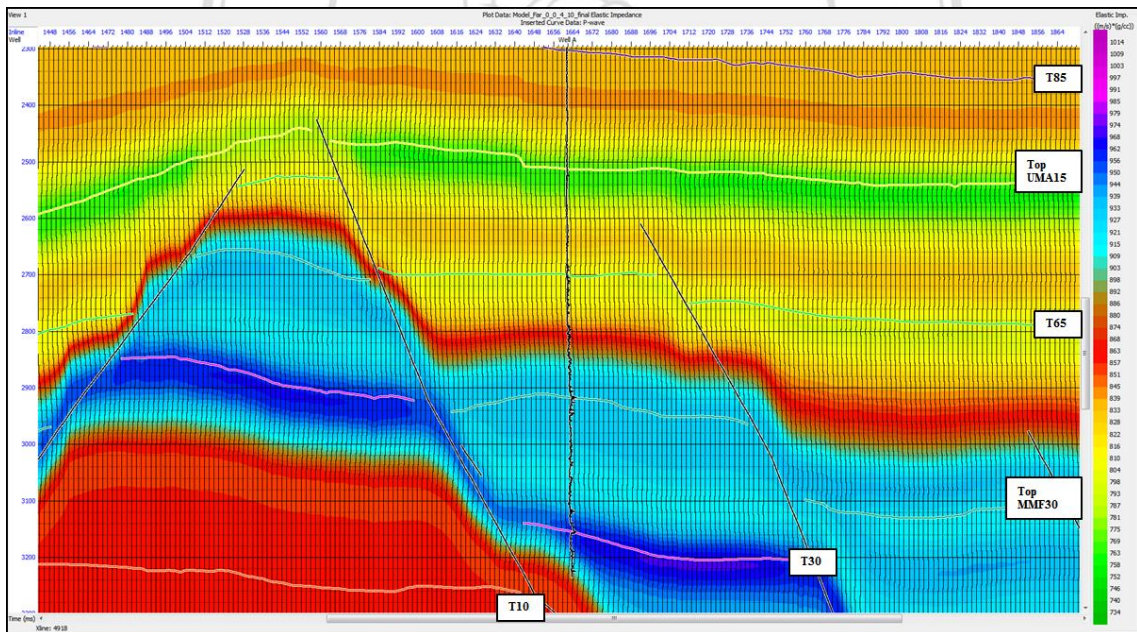


Figure 6.14: Initial strata model for far angle stack (Xline 4918).

After the initial models are generated for near, mid and far angle stacks. These models are used as the input model for post stack inversion. The wavelets that used for inversion process are the wavelets that were extracted after well to seismic tie process for each angle stacks as shown in chapter 5. The post stack inversion is carried out for the whole volume of each angle stacks and separated to three inversion processes for the near, mid and far angle stacks. Figures 6.15 to 6.17 show the results of the inversion

processes at Xline 4918 while Figures 6.18 to 6.20 show the results of the inversion processes at Inline 1662. The elastic impedance inversion of the near, mid and far angle seismic cubes supports the elastic impedance parameters at 6.5 degrees, 19.5 degrees and 33 degrees accordingly. The near, mid and far elastic impedance (EI) logs that calculated from logs dataset are also posted together with inverted seismic volumes at well A location. The EI\_near, EI\_mid and EI\_far logs are filtered by high cut frequencies of 50/60 Hz to match with the low frequencies in inverted seismic volumes. It is noticeable that the EI logs are highly match with the inverted seismic volumes and the low elastic impedance of two the sand reservoir intervals UMA15 and MMF30 in this study are distinguished easily with high elastic impedance of surrounding shale in both logs data and inverted seismic volumes. However, it also shows that there are some low elastic impedance intervals in the logs that indicate some sandstone intervals that could not be seen in inverted seismic volumes due to the difference in frequencies between very high frequency logs data and low frequency seismic data.

Figure 6.21 shows the inverted near, mid and far angle stack volumes at the Well A location, it is obvious that there are huge differences in elastic impedance between inverted seismic volume that represents in colors. Two reservoirs UMA15 and MMF30 are identified clearly in the inverted far angle stack volume rather than in near and mid angle stack volumes. This is because of the AVO response effects in both two reservoirs intervals.

ลิขสิทธิ์มหาวิทยาลัยเชียงใหม่  
Copyright© by Chiang Mai University  
All rights reserved



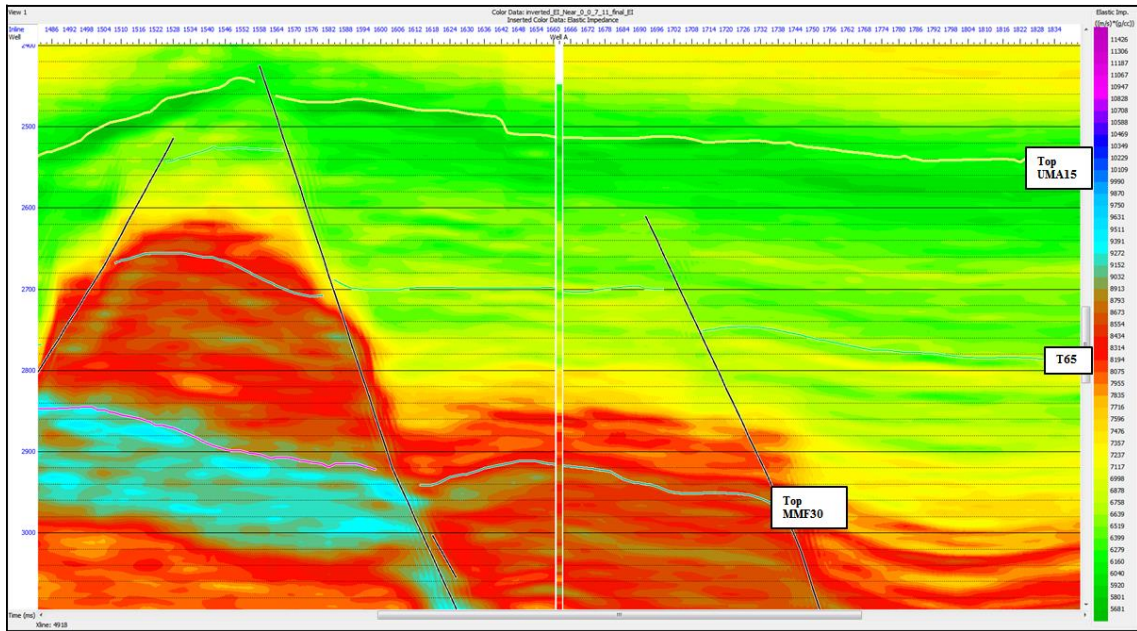


Figure 6.15: Inverted near angle stack volumes (Xline 4918).

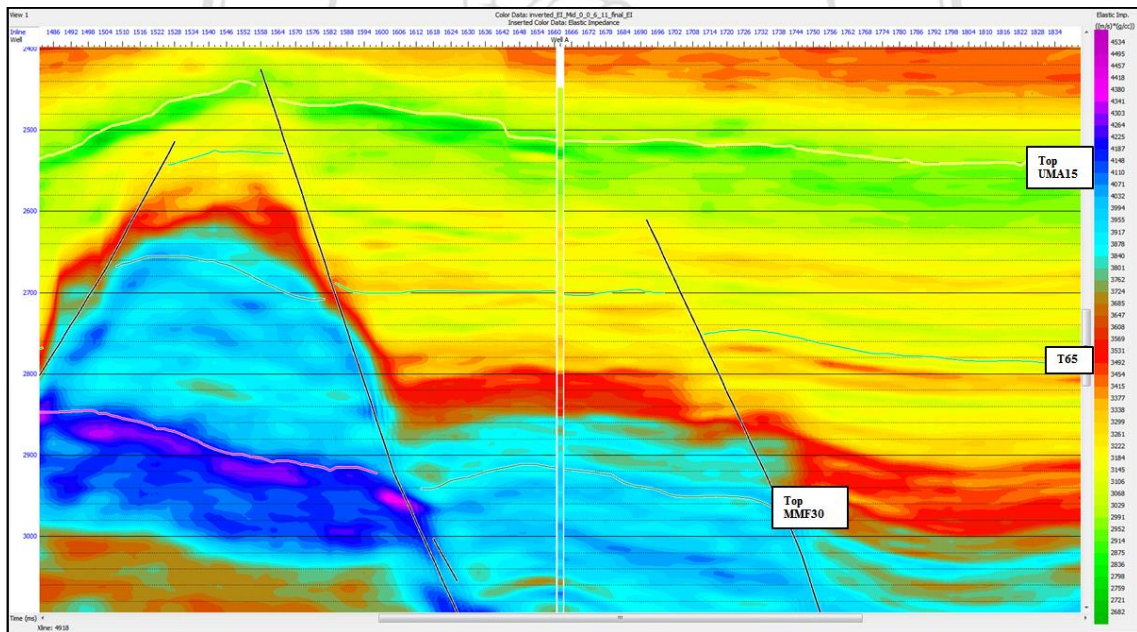


Figure 6.16: Inverted mid angle stack volumes (Xline 4918).

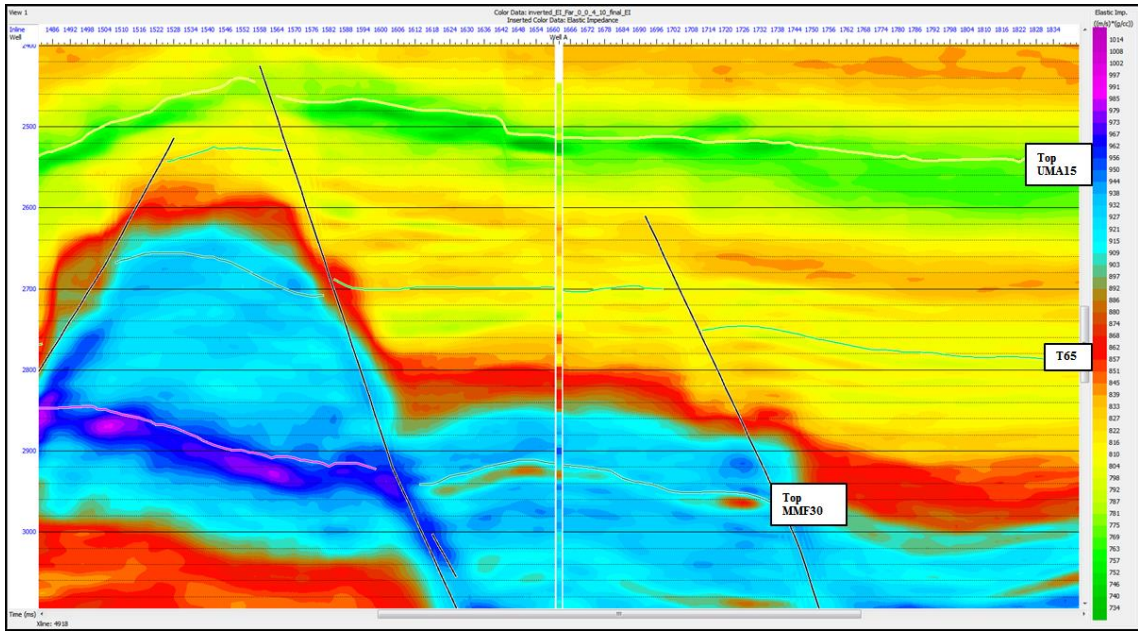


Figure 6.17: Inverted far angle stack volume (Xline 4918).

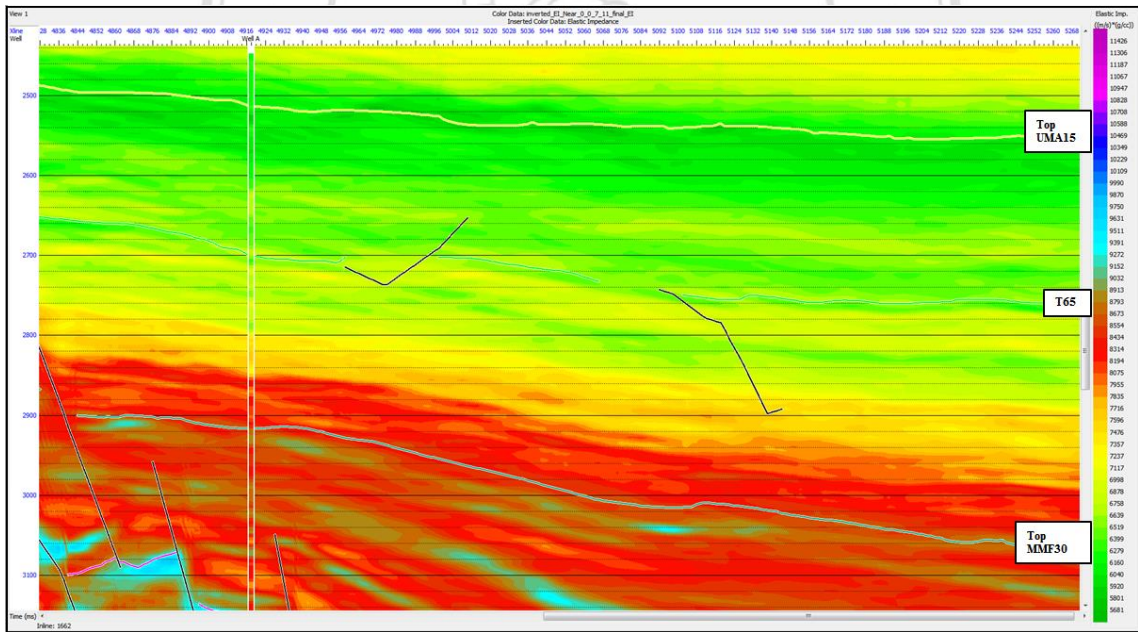


Figure 6.18: Inverted near angle stack volume (Inline 1662).



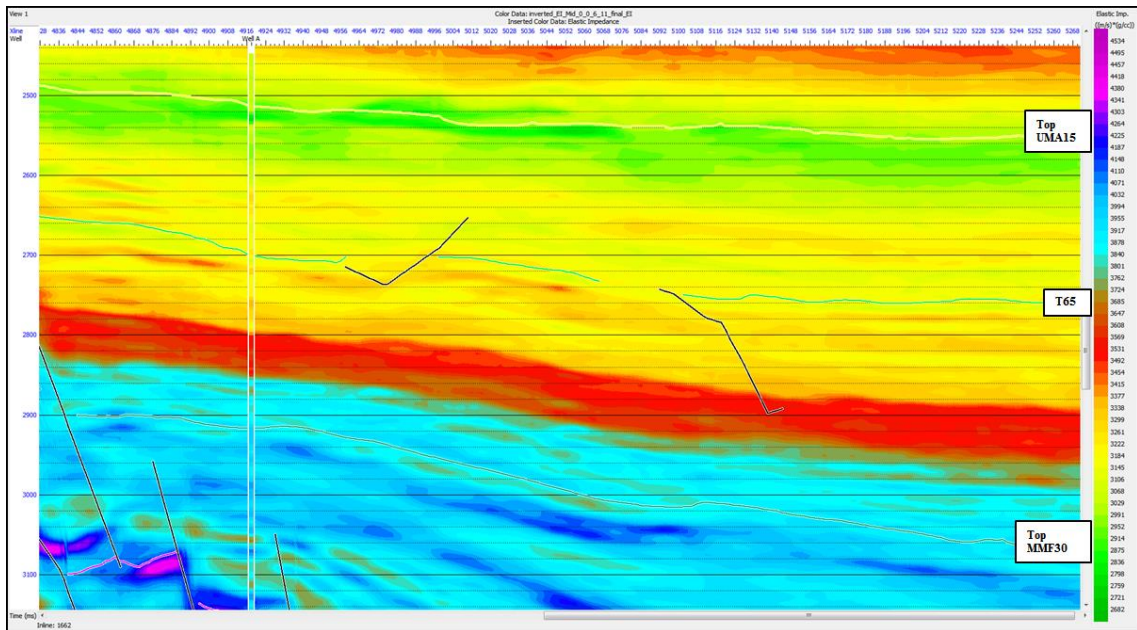


Figure 6.19: Inverted mid angle stack volume (Inline 1662).

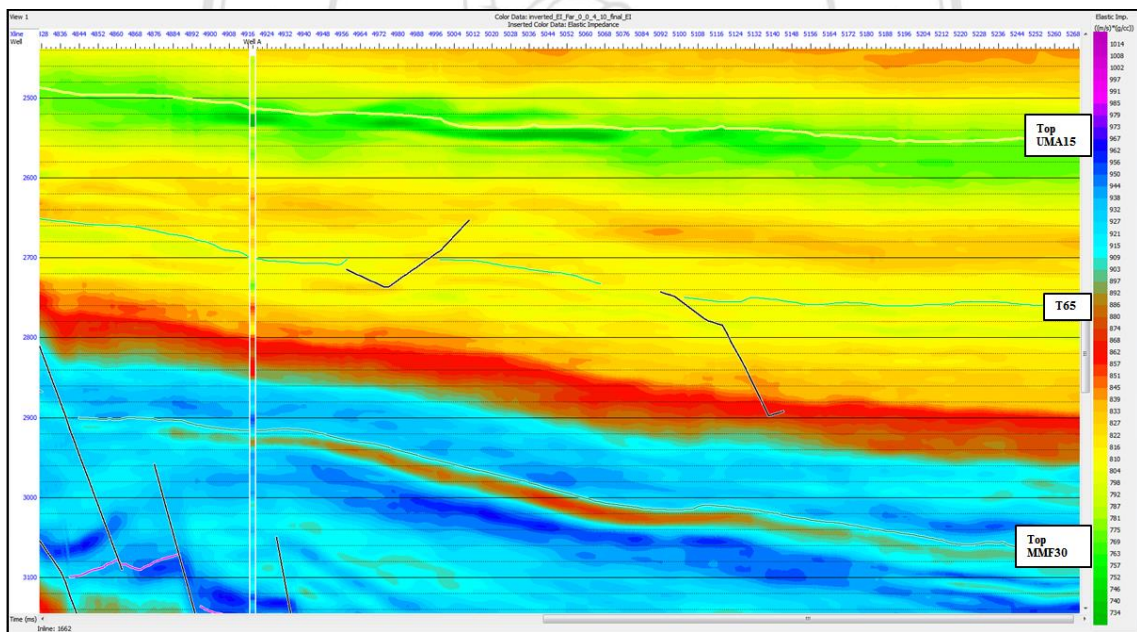


Figure 6.20: Inverted far angle stack volume (Inline 1662).

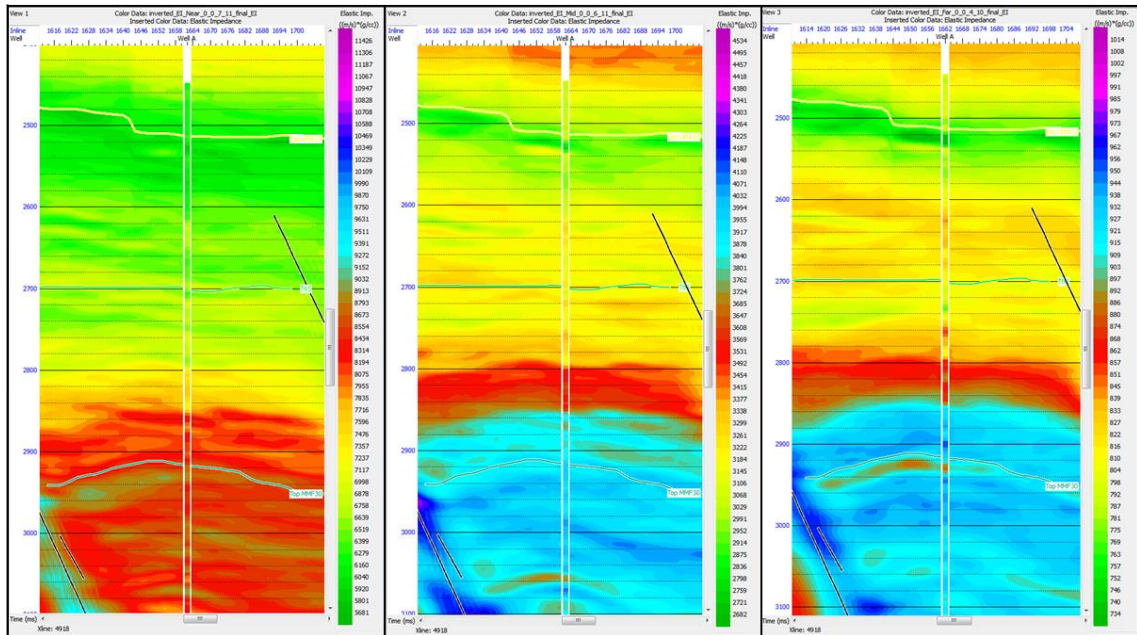


Figure 6.21: Comparison of three elastic impedance volumes at the Well A location (Xline 4918). (from left to right) near, mid and far inverted seismic volume.

In order to quality control the inverted results, the EI\_far log (33 degrees) is plotted overlain on the inverted 33 degrees far angle stack seismic volume (Figure 6.22). This is an advantage of EI inversion because EI allows the well data to be tied directly to the high angle stack seismic without reference to the near angle stack seismic. It is clearly that the EI\_far log shows a strongly correlation with the inverted seismic traces for both reservoir intervals.

After achieving the inverted seismic volumes for near, mid and far angle stacks, the inversion results are then cross plotted in order to highlight AVO anomalies zones in the inverted seismic data. Note that AVO anomalies zones are identified and highlighted in the logs data before and have been mentioned above in this chapter. The AVO anomalies zones identified from logs are then used in the cross plot of inverted angle stack volumes to highlight the high amplitude AVO anomalies zones in the seismic sections. Figures 6.23 and 6.24 show the cross plots of inverted EI\_near volume and inverted EI\_far volume and interest AVO anomalies zones in the seismic sections. Only the results of inverted EI\_near volume and inverted EI\_far volume for two reservoirs UMA15 and MMF30 are cross plotted because they provide the good results rather than

either cross plot of inverted EI\_near volume versus inverted EI\_mid volume or inverted EI\_mid volume versus inverted EI\_far volume.

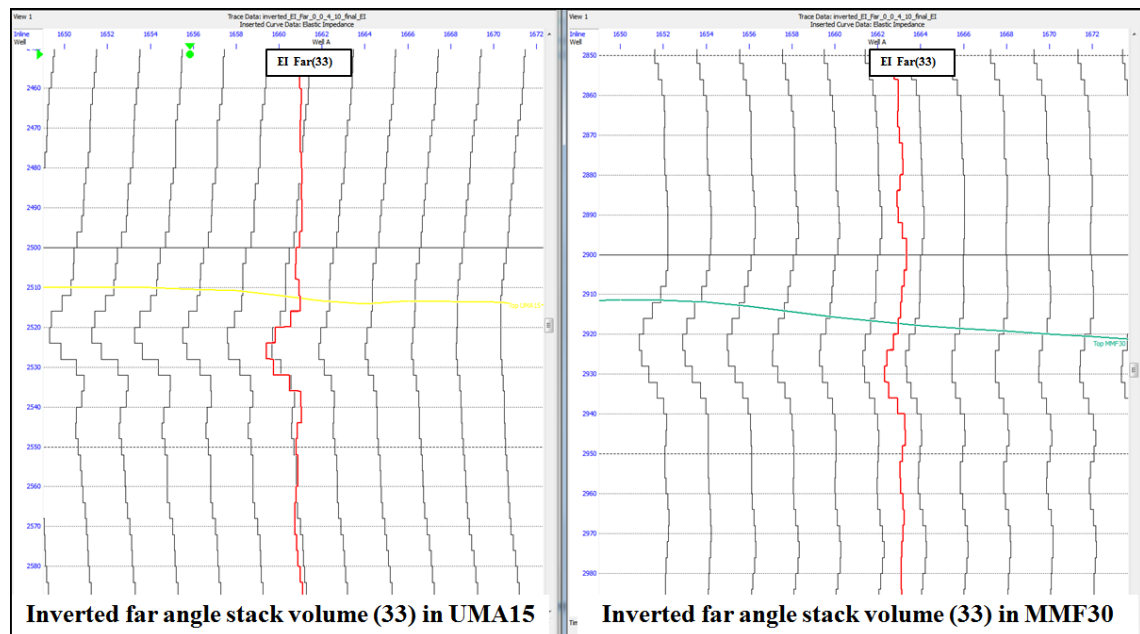


Figure 6.22: Plot of EI\_far log at 33 degrees versus inverted seismic EI\_far volume in two main reservoirs UMA15 and MMF30 in the Well A.

The range of data in the cross plots of each cross plot are 100 ms above and under the horizon Top UMA15 (top of UMA15 reservoir) and about 100 ms above and under the horizon Top MMF30 (top of MMF30 reservoir). The red zones in the cross plots represent high amplitude AVO anomalies zones while the blue zones in the cross plots represents normal AVO zones. The red and blue zone in the cross plots are highlighted in the seismic section. It is obvious that the red color in the seismic section indicates the low elastic impedance areas which could be potential reservoirs in the study area. Meanwhile, the blue color in the seismic section indicates the surrounding rocks that have relative low to high elastic impedance.



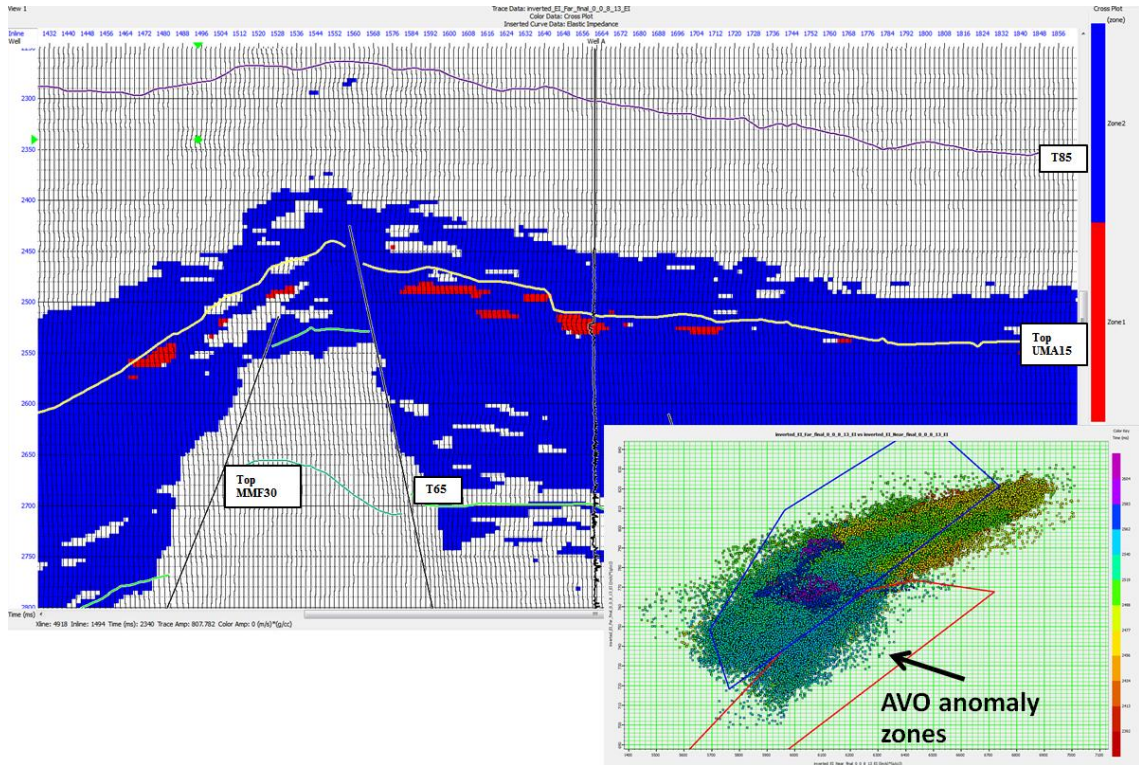


Figure 6.23: Cross section and cross plot of Inverted EI\_near and Inverted EI\_far for the UMA15 reservoir. Note that the cross plot blue and red polygons have already defined from cross plots of EI\_near log and EI\_far log.



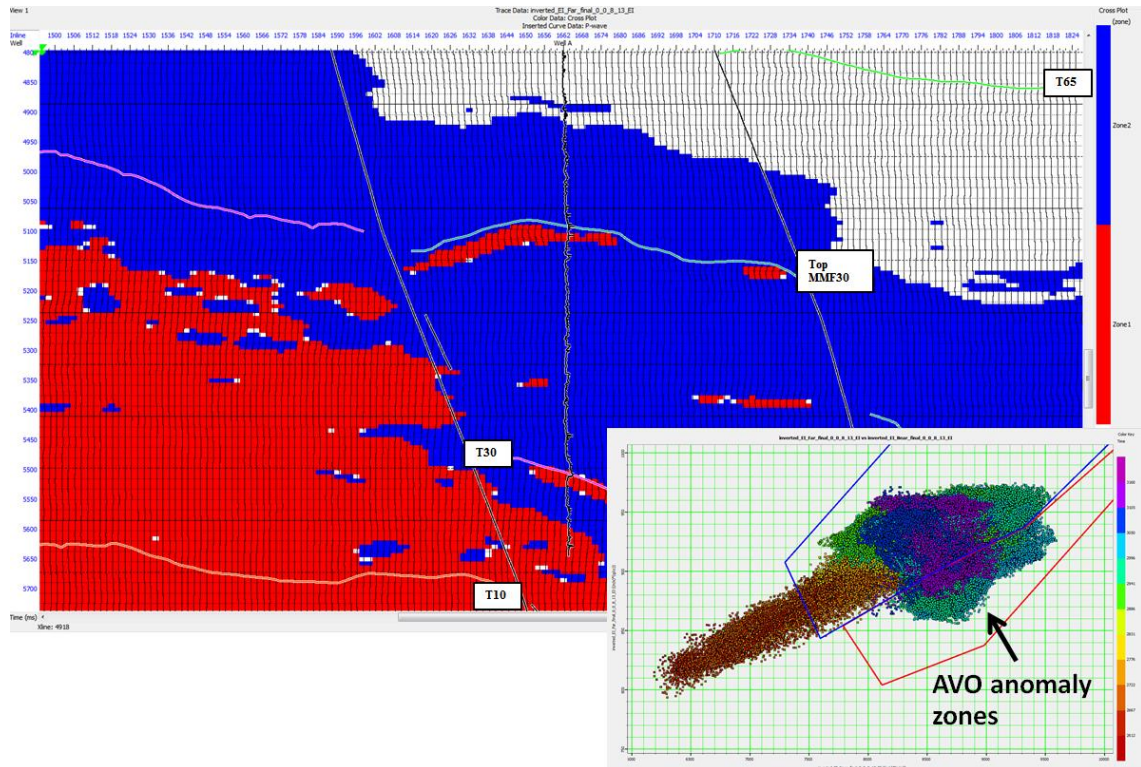


Figure 6.24: Cross section and cross plot of Inverted EI\_near and Inverted EI\_far for the MMF30 reservoir. Note that the cross plot blue and red polygons have already defined from cross plots of EI\_near log and EI\_far log.

In summary, by cross plotting inverted elastic impedance parameters of near angle stack volume versus far angle stack volume, the potential prospects are identified around the well A. Further, this provides information where hydrocarbon can accumulate in the study area. Figures 6.25 and 6.26 show the map of potential hydrocarbon distribution along horizon top UMA15 and horizon top MMF30 respectively. The red zones which indicate AVO anomalies zones that can be potential reservoirs in the seismic section above are mapped along two horizons with the time window of 15 ms under the horizons. Meanwhile the blue zones indicate AVO normal trend. The two maps provide location where elastic impedance is low not only around the Well A location but also throughout all study area. Therefore, it contributes in planning more wells for improving hydrocarbon production in the future.

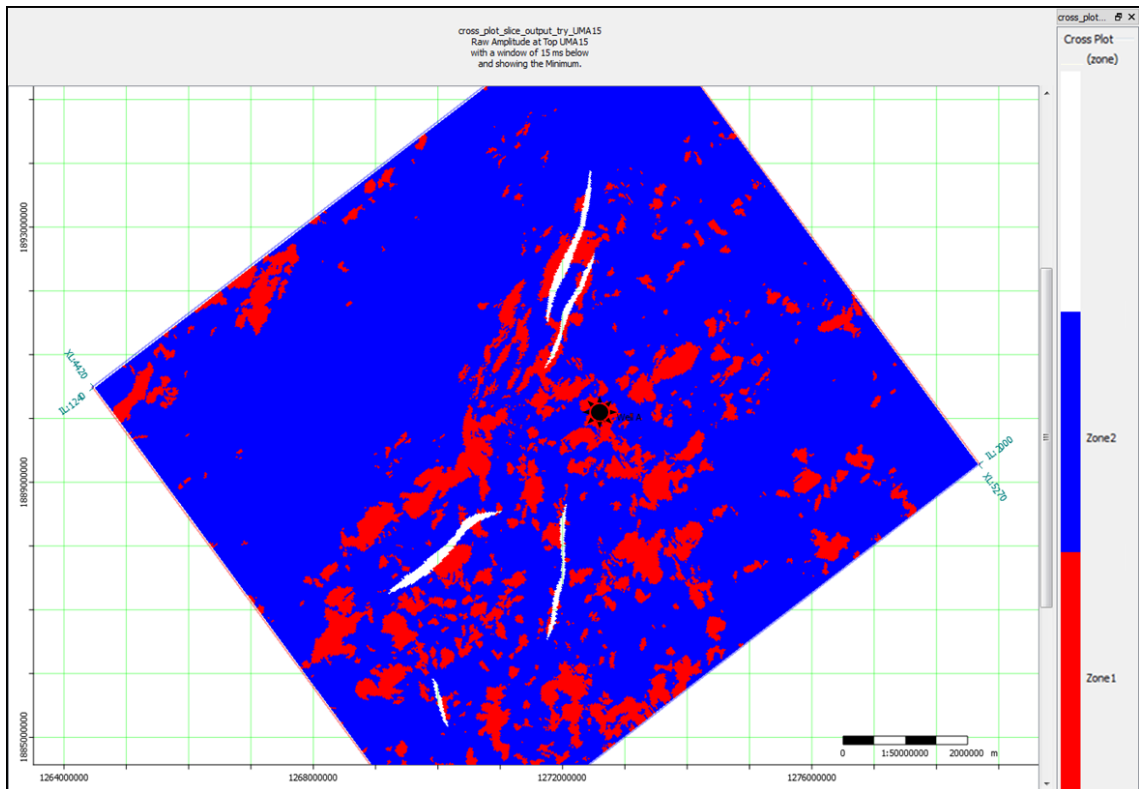


Figure 6.25: Map of potential hydrocarbon distribution along horizon UMA15.

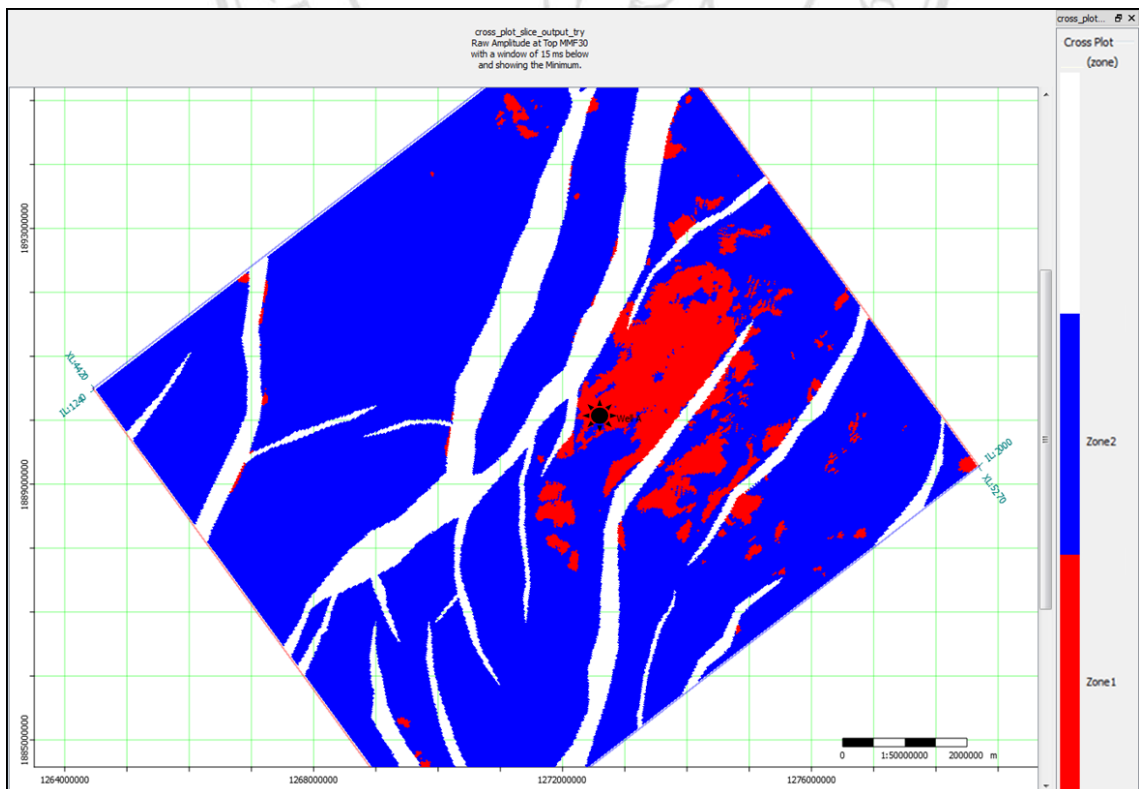


Figure 6.26: Map of potential hydrocarbon distribution along horizon MMF30.